was estimated to be 5×10^{16} m^{-2} on the basis of the spacing between the neighboring partials and λ. This is two orders of magnitude higher than that of the preexisting dislocations and the lattice dislocations stored in the coarse twins. Such a finding suggests that decreasing the twin thickness facilitates the dislocation-TB interactions and affords more room for storage of dislocations, which sustain more pronounced strain hardening in the nt-Cu (*26*, *27*).

These observations suggest that the strain-hardening behavior of nt-Cu samples is governed by two competing processes: dislocation-dislocation interaction hardening in coarse twins, and dislocation-TB interaction hardening in fine twins. With a refining of λ, the contribution from the latter mechanism increases and eventually dominates the strain hardening, as revealed by the continuous increase of *n* values (Fig. 3B). However, the former hardening mechanism usually leads to an inverse trend, diminishing with size refinement (*17*).

Twins are not uncommon in nature, and they appear in various metals and alloys with different crystallographic structures. Extremely thin twin lamellae structures can possibly be achieved under proper conditions during crystal growth, plastic deformation, phase transformations, or thermal annealing of deformed structures. Our finding of the twin thickness giving maximum strength illustrates that the scale-dependent nature of plastic deformation of nanometer-scale materials is not necessarily related to grain boundary–mediated processes. This finding also provides insight into the development of advanced nanostructured materials.

References and Notes

1. E. O. Hall, *Proc. Phys. Soc. London Ser. B* **64**, 747 (1951).
2. N. J. Petch, *J. Iron Steel Inst.* **174**, 25 (1953).
3. J. Schiøtz, K. W. Jacobsen, *Science* **301**, 1357 (2003).
4. S. Yip, *Nature* **391**, 532 (1998).
5. M. A. Meyers, A. Mishra, D. J. Benson, *Prog. Mater. Sci.* **51**, 427 (2006).
6. P. G. Sanders, J. A. Eastman, J. R. Weertman, *Acta Mater.* **45**, 4019 (1997).
7. C. C. Koch, K. M. Youssef, R. O. Scattergood, K. L. Murty, *Adv. Eng. Mater.* **7**, 787 (2005).
8. L. Lu *et al.*, *Acta Mater.* **53**, 2169 (2005).
9. Y. F. Shen, L. Lu, Q. H. Lu, Z. H. Jin, K. Lu, *Scr. Mater.* **52**, 989 (2005).
10. X. Zhang *et al.*, *Acta Mater.* **52**, 995 (2004).
11. L. Lu, Y. Shen, X. Chen, L. Qian, K. Lu, *Science* **304**, 422 (2004); published online 18 March 2004 (10.1126/science.1092905).
12. J. Chen, L. Lu, K. Lu, *Scr. Mater.* **54**, 1913 (2006).
13. S. Cheng *et al.*, *Acta Mater.* **53**, 1521 (2005).
14. Y. Champion *et al.*, *Science* **300**, 310 (2003).
15. Y. M. Wang *et al.*, *Scr. Mater.* **48**, 1851 (2003).
16. A. Misra, X. Zhang, D. Hammon, R. G. Hoagland, *Acta Mater.* **53**, 221 (2005).
17. M. A. Meyers, K. K. Chawla, in *Mechanical Behavior of Materials*, M. Horton, Ed. (Prentice Hall, Upper Saddle River, NJ, 1999), pp. 112–135.
18. Z. H. Jin *et al.*, *Scr. Mater.* **54**, 1163 (2006).
19. X. H. Chen, L. Lu, K. Lu, *J. Appl. Phys.* **102**, 083708 (2007).
20. X. Huang, N. Hansen, N. Tsuji, *Science* **312**, 249 (2006).
21. Z. W. Shan, R. K. Mishra, S. A. Syed Asif, O. L. Warren, A. M. Minor, *Nat. Mater.* **7**, 115 (2008).
22. K. Konopka, J. Mizera, J. W. Wyrzykowski, *J. Mater. Process. Technol.* **99**, 255 (2000).
23. Y. S. Li, N. R. Tao, K. Lu, *Acta Mater.* **56**, 230 (2008).
24. S. I. Rao, P. M. Hazzledine, *Philos. Mag. A* **80**, 2011 (2000).
25. Z. H. Jin *et al.*, *Acta Mater.* **56**, 1126 (2008).
26. M. Dao, L. Lu, Y. Shen, S. Suresh, *Acta Mater.* **54**, 5421 (2006).
27. T. Zhu, J. Li, A. Samanta, H. G. Kim, S. Suresh, *Proc. Natl. Acad. Sci. U.S.A.* **104**, 3031 (2007).

28. Supported by National Natural Science Foundation of China grants 50431010, 50621091, 50725103, and 50890171, Ministry of Science and Technology of China grant 2005CB623604, and the Danish National Research Foundation through the Center for Fundamental Research: Metal Structures in Four Dimensions (X.H.). We thank N. Hansen, Z. Jin, W. Pantleon, and B. Ralph for stimulating discussions, X. Si and H. Ma for sample preparation, S. Zheng for TEM observations, and Y. Shen for conducting some of the tensile tests.

Supporting Online Material

www.sciencemag.org/cgi/content/full/323/5914/607/DC1
Materials and Methods
Table S1
References

24 October 2008; accepted 30 December 2008
10.1126/science.1167641

Control of Graphene's Properties by Reversible Hydrogenation: Evidence for Graphane

D. C. Elias,[1]* R. R. Nair,[1]* T. M. G. Mohiuddin,[1] S. V. Morozov,[2] P. Blake,[3] M. P. Halsall,[1] A. C. Ferrari,[4] D. W. Boukhvalov,[5] M. I. Katsnelson,[5] A. K. Geim,[1,3] K. S. Novoselov[1]†

Although graphite is known as one of the most chemically inert materials, we have found that graphene, a single atomic plane of graphite, can react with atomic hydrogen, which transforms this highly conductive zero-overlap semimetal into an insulator. Transmission electron microscopy reveals that the obtained graphene derivative (graphane) is crystalline and retains the hexagonal lattice, but its period becomes markedly shorter than that of graphene. The reaction with hydrogen is reversible, so that the original metallic state, the lattice spacing, and even the quantum Hall effect can be restored by annealing. Our work illustrates the concept of graphene as a robust atomic-scale scaffold on the basis of which new two-dimensional crystals with designed electronic and other properties can be created by attaching other atoms and molecules.

Graphene, a flat monolayer of carbon atoms tightly packed into a honeycomb lattice, continues to attract immense interest, mostly because of its unusual electronic properties and effects that arise from its truly atomic thickness (*1*). Chemical modification of graphene has been less explored, even though research on carbon nanotubes suggests that graphene can be altered chemically without breaking its resilient C-C bonds. For example, graphene oxide is graphene densely covered with hydroxyl and other groups (*2*–*6*). Unfortunately, graphene oxide is strongly disordered, poorly conductive, and difficult to reduce to the original state (*6*). However, one can imagine atoms or molecules being attached to the atomic scaffold in a strictly periodic manner, which should result in a different electronic structure and, essentially, a different crystalline material. Particularly elegant is the idea of attaching atomic hydrogen to each site of the graphene lattice to create graphane (*7*), which changes the hybridization of carbon atoms from sp^2 into sp^3, thus removing the conducting π-bands and opening an energy gap (*7*, *8*).

Previously, absorption of hydrogen on graphitic surfaces was investigated mostly in conjunction with hydrogen storage, with the research focused on physisorbed molecular hydrogen (*9*–*11*). More recently, atomic hydrogen chemisorbed on carbon nanotubes has been studied theoretically (*12*) as well as by a variety of experimental techniques including infrared (*13*), ultraviolet (*14*, *15*), and x-ray (*16*) spectroscopy and scanning tunneling microscopy (*17*). We report the reversible hydrogenation of single-layer graphene and observed dramatic changes in its transport properties and in its electronic and atomic structure, as evidenced by Raman spectroscopy and transmission electron microscopy (TEM).

Graphene crystals were prepared by use of micromechanical cleavage (*18*) of graphite on top of an oxidized Si substrate (300 nm SiO_2) and then identified by their optical contrast (*1*, *18*) and distinctive Raman signatures (*19*). Three types of samples were used: large (>20 μm) crystals for Raman studies, the standard Hall bar devices 1 μm in width (*18*), and free-standing membranes (*20*, *21*) for TEM. For details of sample fabrication, we refer to earlier work (*18*, *20*, *21*).

[1]School of Physics and Astronomy, University of Manchester, M13 9PL, Manchester, UK. [2]Institute for Microelectronics Technology, 142432 Chernogolovka, Russia. [3]Manchester Centre for Mesoscience and Nanotechnology, University of Manchester, M13 9PL, Manchester, UK. [4]Department of Engineering, Cambridge University, 9 JJ Thomson Avenue, Cambridge CB3 OFA, UK. [5]Institute for Molecules and Materials, Radboud University Nijmegen, 6525 ED Nijmegen, Netherlands.

*These authors contributed equally to this work.
†To whom correspondence should be addressed. E-mail: Kostya@manchester.ac.uk

We first annealed all samples at 300°C in an argon atmosphere for 4 hours in order to remove any possible contamination (for example, resist residues). After their initial characterization, the samples were exposed to a cold hydrogen plasma. We used a low-pressure (0.1 mbar) hydrogen-argon mixture (10% H_2) with dc plasma ignited between two aluminum electrodes. The samples were kept 30 cm away from the discharge zone in order to minimize any possible damage by energetic ions. We found that it typically required 2 hours of plasma treatment to reach the saturation in measured characteristics. As a reference, we used graphene samples exposed to a pure Ar plasma under the same conditions, which showed little changes in their transport and Raman properties (*22*).

Typical changes induced by the hydrogenation in electronic properties of graphene are illustrated in Fig. 1. Before plasma exposure, our devices exhibited the standard ambipolar field effect with the neutrality point (NP) near zero gate voltage (*18*). For the device shown in Fig. 1, mobility μ of charge carriers was ≈14,000 $cm^2 V^{-1} s^{-1}$. This device exhibits a weak temperature dependence of its resistivity at all gate voltages (not visible on the scale of Fig. 1A). We observed metallic dependence close to the NP below 50 K (*23*) and the half-integer quantum Hall effect (QHE) at cryogenic temperatures (Fig. 1B), both of which are hallmarks of single-layer graphene [(*1*) and references therein].

This behavior completely changed after the devices were treated with atomic hydrogen (Fig. 1, C and D). The devices exhibited an insulating behavior such that the resistivity ρ grew by two orders of magnitude with decreasing temperature T from 300 to 4 K (Fig. 1C). Carrier mobility decreased at liquid-helium temperatures down to values of ~10 $cm^2 V^{-1} s^{-1}$ for typical carrier concentrations n of the order of 10^{12} cm^{-2}. The quantum Hall plateaus, so marked in the original devices, completely disappeared, with only weak signatures of Shubnikov–de-Haas oscillations remaining in magnetic field B of 14 T (Fig. 1D). In addition, we observed a shift of NP to gate voltages $V_g \approx +50$ V, which showed that graphene became doped with holes in concentration of $\approx 3 \times 10^{12}$ cm^{-2} (probably due to adsorbed water). At carrier concentrations of less than 3×10^{12} cm^{-2}, the observed temperature dependences ρ(T) can be well fitted by the function $\exp[(T_0/T)^{1/3}]$ (T_0 is the parameter that depends on V_g) (Fig. 2), which is a signature of variable-range hopping in two dimensions (*24*). T_0 exhibits a maximum at NP of ~250 K and strongly decreases away from NP (Fig. 2B). At $n > 4 \times 10^{12}$ cm^{-2} (for both electrons and holes), changes in ρ with T became small (similar to those in pristine graphene), which indicates a transition from the insulating to the metallic regime.

The hydrogenated devices were stable at room T for many days and showed the same characteristics during repeated measurements. However, we could restore the original metallic state by annealing (we used 450°C in Ar atmosphere for 24 hours; higher annealing T damaged graphene). After the annealing, the devices returned practically to the same state as before hydrogenation: ρ as a function of V_g reached again a maximum value of $\approx h/4e^2$, where h is Planck's constant and e is the electron charge, and became only weakly T-dependent (Figs. 1E and 2). Also, μ recovered to ~3500 $cm^2 V^{-1} s^{-1}$, and the QHE reappeared (Fig. 1F). Still, the recovery was not complete: Graphene remained p-doped, the QHE did not restore at filling factors ν larger than ±2 (compare Figure 1, B and F), and zero–B field conductivity σ (=1/ρ) became a sublinear function of n, which indicates an increased number of short-range scatterers (*23*). We attribute the remnant features to vacancies induced by plasma damage or residual oxygen during annealing. To this end, after annealing, the distance (as a function of V_g) between

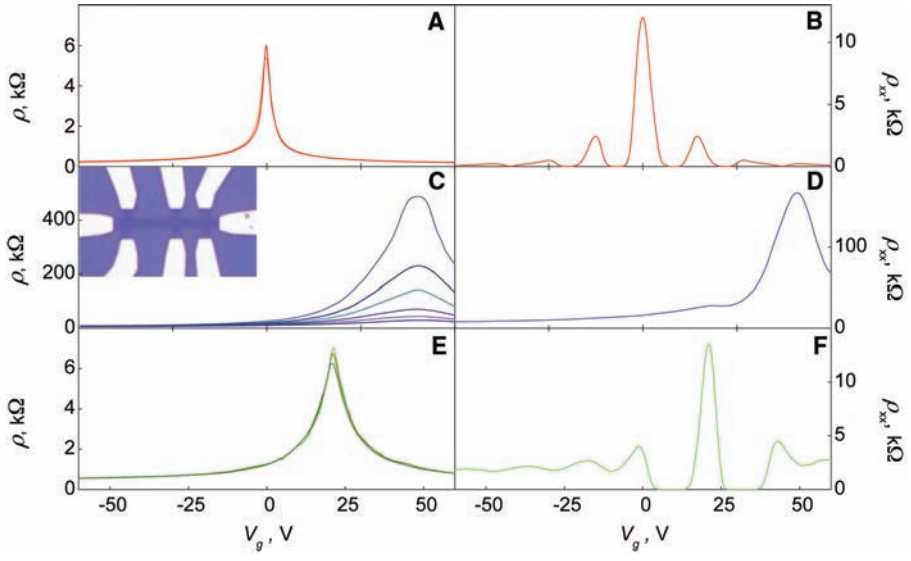

Fig. 1. Control of the electronic properties of graphene by hydrogenation. The electric field effect for one of our devices at zero B at various temperatures T (left column) and in B = 14 T at 4 K (right). (**A** and **B**) The sample before its exposure to atomic hydrogen; curves in (A) for three temperatures (40, 80, and 160 K) practically coincide. (**C** and **D**) After atomic hydrogen treatment. In (C), temperature increases from the top; T = 4, 10, 20, 40, 80, and 160 K. (**E** and **F**) The same sample after annealing. (E) T = 40, 80, and 160 K, from top to bottom. (Inset) Optical micrograph of a typical Hall bar device. The scale is given by its width of 1 μm.

Fig. 2. Metal-insulator transition in hydrogenated graphene. (**A**) Temperature dependence of graphene's resistivity at NP for the sample shown in Fig. 1. Red circles, blue squares, and green triangles are for pristine, hydrogenated, and annealed graphene, respectively. The solid line is a fit by the variable-range hopping dependence $\exp[(T_0/T)^{1/3}]$. (**B**) Characteristic exponents T_0 found from this fitting at different carrier concentrations.

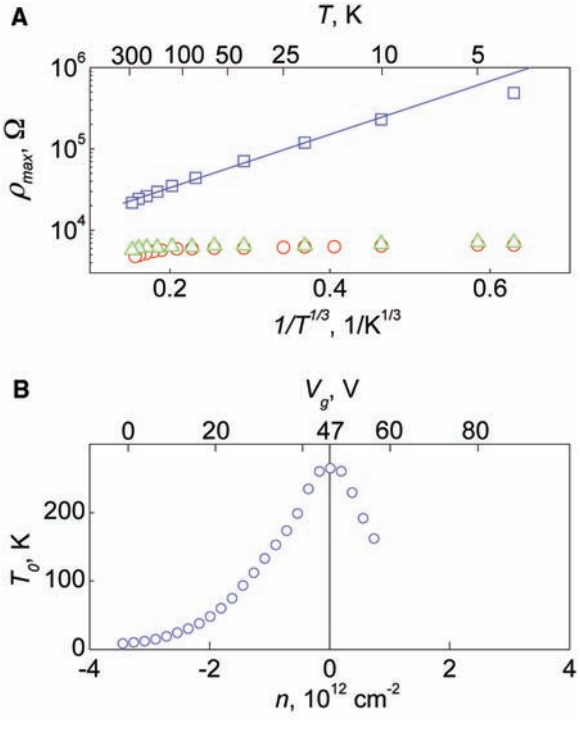

the peaks in ρ_{xx} at $\nu = 0$ and $\nu = \pm 4$ became notably greater (~40%) than that between all the other peaks for both annealed and original devices. The greater distance indicates the presence of mid-gap states (*25*) [such as vacancies (*26*)] that were induced during the processing, which was in agreement with the observed sublinear behavior of the conductivity. The extra charge required to fill these states (*25*) yields their density as of about 1×10^{12} cm^{-2} (with an average spacing of ≈10 nm).

The changes induced by hydrogenation have been corroborated by Raman spectroscopy. The main features in the Raman spectra of carbon-based materials are the G and D peaks that lie at around 1580 and 1350 cm^{-1}, respectively. The G peak corresponds to optical E_{2g} phonons at the Brillouin zone center, whereas the D peak is caused by breathing-like modes (corresponding to transverse optical phonons near the K point) and requires a defect for its activation via an intervalley double-resonance Raman process (*19*, *27*–*29*). Both the G and D peaks arise from vibrations of sp^2-hybridized carbon atoms. The D peak intensity provides a convenient measure for the amount of disorder in graphene (*27*–*29*). Its overtone, the 2D peak, appears around 2680 cm^{-1} and its shape identifies monolayer graphene (*19*). The 2D peak is present even in the absence of any defects because it is the sum of two phonons with opposite momentum. In Fig. 3, there is also a peak at ~1620 cm^{-1}, called D′, which occurs via an intravalley double-resonance process in the presence of defects.

Figure 3A shows the evolution of Raman spectra for graphene crystals that are hydrogenated and annealed simultaneously with the device in Fig. 1 (the use of different samples for Raman studies was essential to avoid an obscuring contribution to the D and D′ peaks caused by the edges of the Hall bars, which were smaller than our laser spot size of about 1 μm). Hydrogenation resulted in the appearance of sharp D and D′ peaks, slight broadening and a decrease of the height of the 2D peak relative to the G peak, and the onset of a combination mode (D + D′) around 2950 cm^{-1}, which, unlike the 2D and 2D′ bands, requires a defect for its activation because it is a combination of two phonons with different momentum. The D peak in hydrogenated graphene is observed at 1342 cm^{-1} and is very sharp, as compared with that in disordered or nanostructured carbon-based materials (*29*). We attribute the activation of this sharp D peak in our hydrogenated samples to breaking of the translational symmetry of C-C sp^2 bonds after the formation of C-H sp^3 bonds. Although the majority of carbon bonds in hydrogenated graphene are expected to acquire sp^3 hybridization, we do not expect to see any Raman signature of C-C sp^3 bonds because their cross section at visible light excitation is negligible as compared with that of the resonant C-C sp^2 bonds, and therefore even a small residual sp^2 phase should generally dominate our spectra, as happens in other diamondlike compounds (*22*, *29*).

After annealing, the Raman spectrum recovered to almost its original shape, and all of the

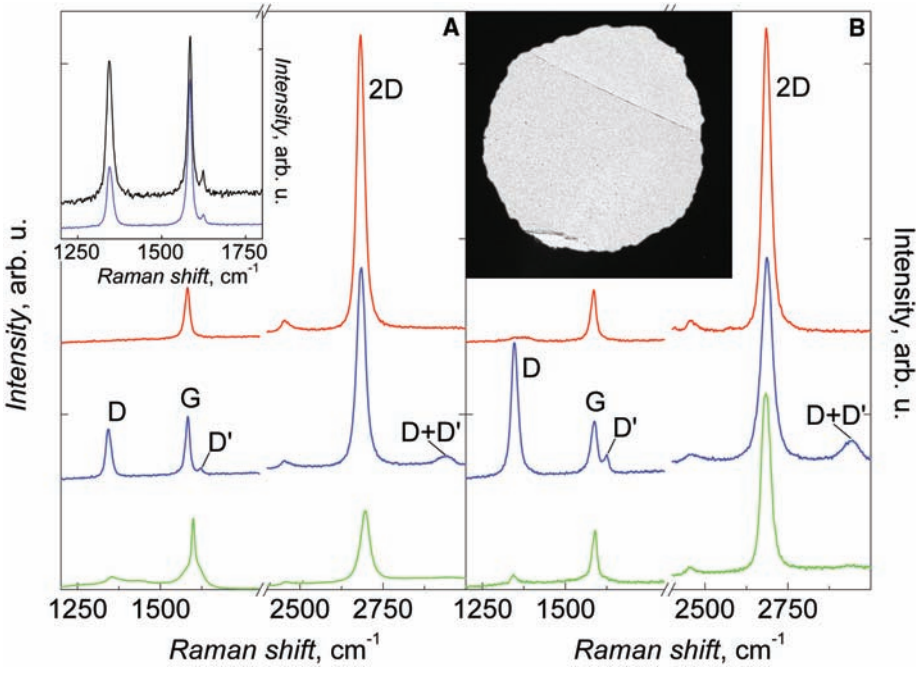

Fig. 3. Changes in Raman spectra of graphene caused by hydrogenation. The spectra are normalized to have a similar intensity of the G peak. (**A**) Graphene on SiO_2. (**B**) Free-standing graphene. Red, blue, and green curves (top to bottom) correspond to pristine, hydrogenated, and annealed samples, respectively. Graphene was hydrogenated for ~2 hours, and the spectra were measured with a Renishaw spectrometer at wavelength 514 nm and low power to avoid damage to the graphene during measurements. (Left inset) Comparison between the evolution of D and D′ peaks for single- and double-sided exposure to atomic hydrogen. Shown is a partially hydrogenated state achieved after 1 hour of simultaneous exposure of graphene on SiO_2 (blue curve) and of a membrane (black curve). (Right inset) TEM image of one of our membranes that partially covers the aperture 50 μm in diameter.

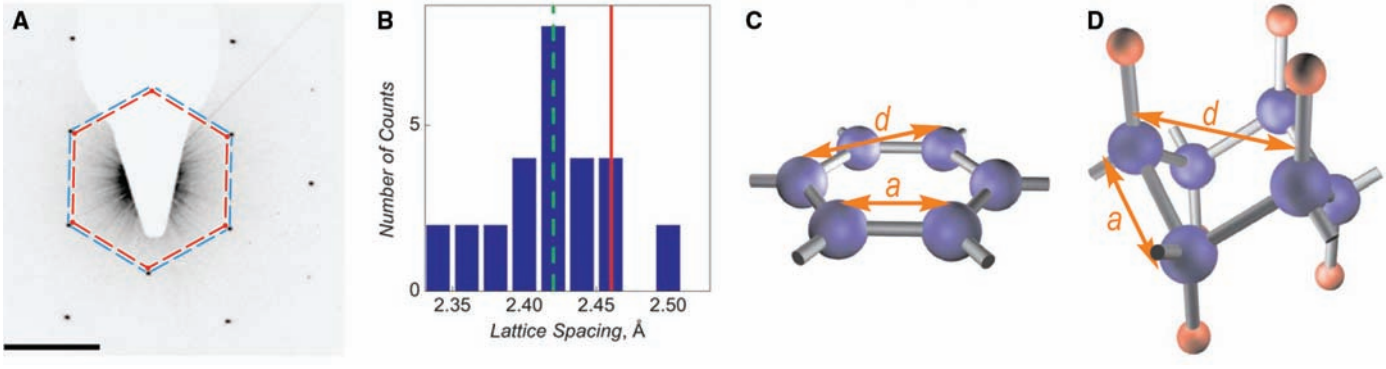

Fig. 4. Structural studies of graphane via TEM [we used a Tecnai F30 (FEI, Eindhoven, the Netherlands)]. (**A**) Changes in the electron diffraction after ~4 hours exposure of graphene membranes to atomic hydrogen. Scale bar, 5 nm^{-1}. The blue hexagon is a guide to the eye and marks positions of the diffraction spots in graphane. The equivalent diffraction spots in graphene under the same conditions are shown by the red hexagon. (**B**) Distribution of the lattice spacing *d* found in hydrogenated membranes. The green dashed line marks the average value, whereas the red solid line shows *d* always observed for graphene (both before hydrogenation and after annealing). (**C** and **D**) Schematic representation of the crystal structure of graphene and theoretically predicted graphane. Carbon atoms are shown as blue spheres, and hydrogen atoms are shown as red spheres.

defect-related peaks (D, D′, and D+D′) were strongly suppressed. However, two broad low-intensity bands appeared, overlapping a sharper G and residual D peaks. These bands are indicative of some residual structural disorder (*29*). The 2D peak remained relatively small with respect to the G peak when compared with the same ratio in the pristine sample, and both became shifted to higher energies, indicating that the annealed graphene is p-doped (*30*). The observed changes in Raman spectra are in broad agreement with our transport measurements.

For graphene on a substrate, only one side is accessible to atomic hydrogen, and the plasma exposure is not expected to result in graphane (which assumes hydrogen atoms attached on both sides). For more effective hydrogenation, we employed free-standing graphene membranes (Fig. 3B, inset) (*20*, *21*). The experiments described below refer to membranes that had some free edges to facilitate the relaxation of strain induced by hydrogenation [membranes with all the sides fixed to a metal scaffold are discussed in (*22*)]. Raman spectra for hydrogenated and subsequently annealed membranes (Fig. 3B) were rather similar to those described above for graphene on SiO_2, but with some notable differences. If hydrogenated simultaneously and before reaching the saturation, the D peak for a membrane was by a factor of two greater than that for graphene on a substrate (Fig. 3A, inset), which indicates the formation of twice as many C-H bonds in the membrane. This result agrees with the general expectation that atomic hydrogen attaches to both sides of membranes. Moreover, the D peak could become up to three times greater than the G peak after prolonged exposures of membranes to atomic hydrogen (Fig. 3B).

Further information about hydrogenated membranes was obtained with TEM. For graphene, the electron-diffraction (ED) patterns observed on dozens of the studied membranes were always the same, exhibiting the hexagonal symmetry with the lattice constant $d = 2.46 \pm 0.02$ Å. Prolonged exposure to atomic hydrogen preserved the hexagonal symmetry and hence crystallinity, but led to drastic changes in the lattice constant d, which could decrease by as much as 5% (Fig. 4A). Generally, the compression was not uniform, and different parts of membranes exhibited locally different in-plane periodicities (Fig. 4B; diameters of the selected area for the ED and studied membranes were 0.3 μm and 30 to 50 μm, respectively). Such nonuniformity is generally not unexpected because the crystals were fixed to the scaffold (Fig. 3) that restricted their isotropic shrinkage. We found that the more extended free edges a membrane had, the more uniformly it became hydrogenated (*22*). In the extreme case of all the edges being fixed to the scaffold, even domains with a stretched lattice could be observed (*22*). Annealing led to complete recovery of the original periodicity observed in TEM.

The in-plane compression of graphene's lattice can only be the result of chemical modification as opposed to physical forces, because any compression that is not stabilized on an atomic scale should cause the membranes to buckle. Furthermore, strains of the order of a few percent would result in massive variations of the Raman peaks, which was not the case. The most obvious candidate for the modified crystal lattice is graphane (*7*, *8*). In this until-now-theoretical material, hydrogen attaches to graphene's sublattices A and B from the two opposite sides, and carbon atoms in A and B move out of the plane ("buckle"), as shown in Fig. 4D. The in-plane periodicity probed by TEM would then substantially shrink if the length a of the C-C bond were to remain the same as in graphene (1.42 Å). However, the change in hybridization from sp^2 to sp^3 generally results in longer C-C bonds, which is the effect opposing to the lattice shrinkage by atomic-scale buckling. Recent calculations (*8*) predicted a in graphane to be ≈1.53 Å (near that of diamond) and the in-plane periodicity d to be ≈1% smaller than in graphene. Although the maximum in the observed distribution of d occurs at ≈2.42 Å (that is, near the theoretical value for graphane) (Fig. 4B), the observation of more compressed areas (such as in Fig. 4A) suggests that the equilibrium d (without strain imposed by the scaffold) should be smaller. The latter implies either shorter or stronger buckled C-C bonds, or both, are present. Alternatively, the experimentally produced graphane may have a more complex hydrogen bonding than the one suggested by theory.

Finally, let us return to the graphene hydrogenated on a substrate (Figs. 1 and 3). Single-sided hydrogenation of ideal graphene would create a material that is thermodynamically unstable (*7*, *8*), and therefore our experiments seem to be in conflict with the theory [for the case of graphene on a substrate, we can exclude the possibility of double-sided hydrogenation because the diffusion of hydrogen along the graphene-SiO_2 interface is negligible (*31*)]. However, realistic graphene samples are not microscopically flat but always rippled (*20*, *21*), which should facilitate their single-sided hydrogenation. Indeed, attached hydrogen is expected to change the hybridization of carbon from sp^2 to (practically) sp^3 with angles of ~110° acquired between all of the bonds (*7*). These constraints necessitate the movement of carbon atoms out of the plane in the direction of the attached hydrogen, at the cost of an increase in elastic energy. However, for a convex surface, the lattice is already deformed in the direction that favors sp^3 bonding, which lowers the total energy. As shown in (*22*), single-sided hydrogenation becomes energetically favorable for a typical size of ripples observed experimentally (*20*). Because of the random nature of ripples, single-sided graphane is expected to be a disordered material, similar to graphene oxide, rather than a new graphene-based crystal. The formation of a disordered material also explains the observation of variable-range hopping in our transport experiments. The importance of ripples for hydrogenation of graphene on a substrate is further evidenced in experiments involving bilayer samples, which show a substantially lower level of hydrogenation than monolayers under the same conditions (*22*). We attribute this observation to the fact that bilayer graphene is less rippled (*20*).

The distinct crystal structure of hydrogenated graphene and pronounced changes in its electronic and phonon properties reveal two new graphene derivatives, one crystalline and the other disordered. The results show that conversion of graphene into other giant molecules with a regular structure is possible.

References and Notes

1. A. K. Geim, K. S. Novoselov, *Nat. Mater.* **6**, 183 (2007).
2. S. Stankovich *et al.*, *J. Mater. Chem.* **16**, 155 (2006).
3. S. Stankovich *et al.*, *Nature* **442**, 282 (2006).
4. X. Wang, L. Zhi, K. Mullen, *Nano Lett.* **8**, 323 (2008).
5. S. Gilje, S. Han, M. Wang, K. L. Wang, R. B. Kaner, *Nano Lett.* **7**, 3394 (2007).
6. C. Gomez-Navarro *et al.*, *Nano Lett.* **7**, 3499 (2007).
7. J. O. Sofo, A. S. Chaudhari, G. D. Barber, *Phys. Rev. B* **75**, 153401 (2007).
8. D. W. Boukhvalov, M. I. Katsnelson, A. I. Lichtenstein, *Phys. Rev. B* **77**, 035427 (2008).
9. A. C. Dillon *et al.*, *Nature* **386**, 377 (1997).
10. F. L. Darkrim, P. Malbrunot, G. P. Tartaglia, *Int. J. Hydrogen Energy* **27**, 193 (2002).
11. A. Züttel *et al.*, *Int. J. Hydrogen Energy* **27**, 203 (2002).
12. T. Yildirim, O. Gulseren, S. Ciraci, *Phys. Rev. B* **64**, 075404 (2001).
13. B. N. Khare, M. Meyyappan, A. M. Cassell, C. V. Nguyen, J. Han, *Nano Lett.* **2**, 73 (2002).
14. P. Ruffieux *et al.*, *Phys. Rev. B* **66**, 245416 (2002).
15. D. Neumann *et al.*, *Appl. Phys. A* **55**, 489 (1992).
16. A. Nikitin *et al.*, *Phys. Rev. Lett.* **95**, 225507 (2005).
17. L. Hornekær *et al.*, *Phys. Rev. Lett.* **96**, 156104 (2006).
18. K. S. Novoselov *et al.*, *Science* **306**, 666 (2004).
19. A. C. Ferrari *et al.*, *Phys. Rev. Lett.* **97**, 187401 (2006).
20. J. C. Meyer *et al.*, *Nature* **446**, 60 (2007).
21. T. J. Booth *et al.*, *Nano Lett.* **8**, 2442 (2008).
22. Supporting online material is available on *Science* Online.
23. S. V. Morozov *et al.*, *Phys. Rev. Lett.* **100**, 016602 (2008).
24. N. F. Mott, *Philos. Mag.* **19**, 835 (1969).
25. T. O. Wehling *et al.*, *Nano Lett.* **8**, 173 (2008).
26. V. M. Pereira, F. Guinea, J. M. B. Lopes dos Santos, N. M. R. Peres, A. H. Castro Neto, *Phys. Rev. Lett.* **96**, 036801 (2006).
27. A. C. Ferrari, *Solid State Commun.* **143**, 47 (2007).
28. F. Tuinstra, J. L. Koenig, *J. Chem. Phys.* **53**, 1126 (1970).
29. A. C. Ferrari, J. Robertson, *Phys. Rev. B* **61**, 14095 (2000).
30. A. Das *et al.*, *Nat. Nanotechnol.* **3**, 210 (2008).
31. J. S. Bunch *et al.*, *Nano Lett.* **8**, 2458 (2008).

32. This work was supported by Engineering and Physical Sciences Research Council (UK), the Royal Society, the European Research Council (programs "Ideas" and "New and Emerging Science and Technology," project "Structural Information of Biological Molecules at Atomic Resolution"), Office of Naval Research, and Air Force Research Office of Scientific Research. D.C.E. acknowledges financial support from the National Council for Scientific and Technological Development (Brazil). The authors are grateful to Nacional de Grafite for providing high-quality crystals of natural graphite.

Supporting Online Material

www.sciencemag.org/cgi/content/full/323/5914/610/DC1
SOM Text
Figs. S1 to S7
References

13 October 2008; accepted 10 December 2008
10.1126/science.1167130